



On-chip flow rate sensing via membrane deformation and bistability probed by microwave resonators

Arda Secme^{1,2,3} · Hadi Sedaghat Pisheh^{1,2} · Uzay Tefek^{1,2} · H. Dilara Uslu^{1,2} · Berk Kucukoglu^{1,2} · Ceren Alatas^{1,2} · Mehmet Kelleci^{1,2} · M. Selim Hanay^{1,2,3}

Received: 10 November 2022 / Accepted: 27 March 2023 / Published online: 8 April 2023
© The Author(s), under exclusive licence to Springer-Verlag GmbH Germany, part of Springer Nature 2023

Abstract

Precise monitoring of fluid flow rates constitutes an integral problem in various lab-on-a-chip applications. While off-chip flow sensors are commonly used, new sensing mechanisms are being investigated to address the needs of increasingly complex lab-on-a-chip platforms which require local and non-intrusive flow rate sensing. In this regard, the deformability of microfluidic components has recently attracted attention as an on-chip sensing mechanism. To develop an on-chip flow rate sensor, here we utilized the mechanical deformations of a 220 nm thick Silicon Nitride membrane integrated with the microfluidic channel. Applied pressure and fluid flow induce different modes of deformations on the membrane, which are electronically probed by an integrated microwave resonator. The flow changes the capacitance, and in turn resonance frequency, of the microwave resonator. By tracking the resonance frequency, liquid flow was probed with the device. In addition to responding to applied pressure by deflection, the membrane also exhibits periodic pulsation motion under fluid flow at a constant rate. The two separate mechanisms, deflection and pulsation, constitute sensing mechanisms for pressure and flow rate. Using the same device architecture, we also detected pressure-induced deformations by a gas to draw further insight into the sensing mechanism of the membrane. Flow rate measurements based on the deformation and instability of thin membranes demonstrate the transduction potential of microwave resonators for fluid–structure interactions at micro- and nanoscales.

Keywords Flow rate sensing · Microwave sensors · Microfluidics · Membranes · Fluid–structure interaction · Deformable microfluidics · Nonlinear microfluidics · Nanomembrane flow sensing

1 Introduction

Local flow rate measurements on different fluidic channels constitute a need for various microfluidic applications. With the information provided by flow rates, one can control nutrient and cell concentrations in microscale chambers (Wu et al. 2008; Mehling and Tay 2014), modify cellular

adhesion rates on a substrate (Christ and Turner 2010), and sort particles of different sizes (Zhou et al. 2019). In organ-on-a-chip systems, cells need to be supplied with an optimal flux of nutrients to maintain their vitality (Harink et al. 2013). Furthermore, finely controlled doses of drugs should be administered to test the response of cells from tumor biopsies (Stevens et al. 2016; Cetin et al. 2017). In digital microfluidics, droplets with well-controlled sizes and compositions can only be generated by an exquisite and local control of different flow rates (Ward et al. 2005; Garstecki et al. 2006; Glawdel et al. 2012). In most biomedical reactors, syringe or peristaltic pumps are used to set the flow rates; however, these devices have inherent delays and fluctuations that negatively affect the controllability of such platforms. Commercial flow sensors are readily available, but naturally they are not integrated at the chip scale, impeding their utility for local flow sensing. Robust on-chip flow sensors appear to be the most efficient solution for flow rate measurements for microchannels.

Arda Secme and Hadi Sedaghat Pisheh authors are equal contributors.

✉ M. Selim Hanay
selimhanay@bilkent.edu.tr

¹ Department of Mechanical Engineering, Bilkent University, Ankara 06800, Turkey

² UNAM Institute of Materials Science and Nanotechnology, Bilkent University, Ankara 06800, Turkey

³ Present Address: Department of Applied Physics, California Institute of Technology, Pasadena, CA 91125, USA

Many different mechanisms have been used to develop flow rate sensors for microfluidic applications (Nguyen 1997; Ejeian et al. 2019; Cavaniol et al. 2022). These mechanisms are classified as active and passive sensors depending on whether the sensor supplies energy to the fluid (Cavaniol et al. 2022). Active sensors, based on thermal conductivity and Coriolis force, constitute the majority of the commercial devices. Thermal flow sensors work by heating a region along the channel and the heat transfer rate along the channel is measured to infer fluid speed (Dijkstra et al. 2007; Kuo et al. 2012; Lin and Burns 2015; Baldwin et al. 2016; Kim et al. 2019). Thermal flow sensors do not require any moving parts and are relatively easy to fabricate. However, their operation depends critically on the knowledge of the heat capacity of the fluid, and their accuracy is degraded when the composition of fluid is complex whereby unaccounted channels for heat transfer arise. This dependency could create problems for application where flow composition changes over time. Coriolis flowmeters work by detecting the force perpendicular to the flow direction through an oscillating channel (Enoksson et al. 1997; Haneveld et al. 2010). While these flowmeters attain large dynamic range, they are more complex and expensive compared to thermal flow sensors. In general, active flowmeters have the shortcomings of inducing heat on the liquid and requiring a small fluidic channel diameter to operate.

In passive flow sensing, optical, mechanical and capacitive (electronic) sensors have been predominantly investigated. When direct measurements of flow rates in the channel are required, optical systems could be used. Optical flow meters can be divided into two main categories: particle or Doppler velocimetry. Tracking a microparticle (Salipante et al. 2017) or a microbubble (Chen et al. 2019; Tang et al. 2019) with a microscope and measuring how far the objects move within a certain time-period enables the measurement of flow velocity. In Doppler velocimetry, the moving particle modulates interference fringes with a rate proportional to its velocity (Czarske et al. 2002; Campagnolo et al. 2013; Stern et al. 2014). Similarly, interference patterns arising from two closely spaced cantilevers was fabricated for an optofluidics-based flow sensor (Cheri et al. 2014). Optical sensors generally suffer from the large size and cost of microscope-based imaging systems.

Within passive sensors, mechanical sensors can be measured by compact setups; they also have the advantage of circumventing the need to introduce extra particles into the flow. For mechanical flow rate sensors, cantilevers (Gass et al. 1993; Wexler et al. 2013) and spring-like structures (Attia et al. 2009) were used to measure the drag force in microfluidic channels. A cantilever-based sensor with variable-sized holes was manufactured and flow rate changes were correlated with cantilever deflection (Noeth et al. 2014). This sensor worked by passing the fluid through a

perforated cantilever structure: the deflection of the cantilever was then used to quantify the flow rate. While this system achieved 1 nL/min sensitivity, the flow needs to pass through the delicate mechanical structure which can create an impediment for lab-on-a-chip applications where cells and microparticles are carried by the flow.

In typical capacitive sensing scenarios (Oosterbroek et al. 1999; Temiz and Delamarche 2018; Wissman et al. 2019), the pressure difference between two points along the channel is measured, which is then converted into flow rate. While capacitive sensors offer the advantage of compactness and low-cost due to electronics-integration, they require the knowledge of channel's hydrodynamic resistance to relate the pressure difference to flow rates. Numerous types of electrical flow sensors operating in the radio frequency have been reported (Zarifi et al. 2018; Maenhout et al. 2019; Węglarski et al. 2020). Recently, Zarifi et al. (Zarifi et al. 2018) have developed a non-contact flow rate sensor that exploits the deflection of a thin polydimethylsiloxane (PDMS) layer and measured this deflection using a microwave sensor placed in close proximity. This sensor has reached a sensitivity of 0.5 $\mu\text{L}/\text{min}$, however, the relaxation timescale of the elastomeric PDMS layer resulted in long recovery times (several minutes).

While deformable components were used before for flow sensing in microfluidics, the use of nanoscale-thick membranes along the flow direction (i.e. as a part of channel wall) has not attracted significant attention. This approach has the advantage of simpler fabrication compared to introducing 1D cantilevers within a channel. In this work, we investigated the deformations of a 220 nm Silicon Nitride membrane as it interacts with a fluid (Fig. 1a). The fluid pressure and flow over the membrane creates various types of deformations on the membrane opening up ways for indirect and direct measurements of flow rates. The membrane is embedded in a microfluidic system and forms part of the bottom wall of the microchannel. As the membrane material, we chose Silicon Nitride owing to its desirable mechanical qualities compared to elastomers such as PDMS; this way, we expected to build a robust sensor, which was still compliant owing to its small bending stiffness. The ceramic nature of the membrane increases the sensor durability and enhances its mechanical qualities, such as the ability to measure liquid flow within the microfluidic channel and reaching fast mechanical recovery rates. The deformations of the membrane are probed by microwave electrodes directly placed on the membrane as described below. The liquid flow induces first a sudden deformation on the membrane as the pressure is applied, followed by a periodic instability of the membrane dynamics at a constant flow rate. The initial, sudden deflection of the membrane due to the applied pressure can be used as an indirect means to obtain flow rate for a fixed fluid path geometry. The second effect, periodic instability of the

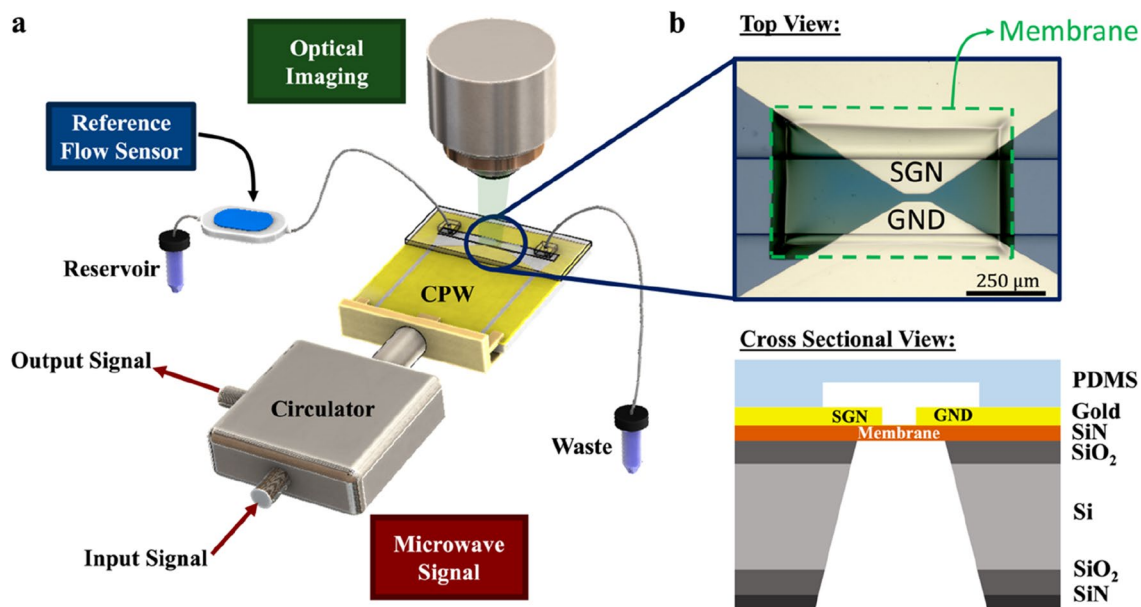


Fig. 1 Experimental Configuration. **a** The chip was placed under a microscope to observe membrane deflections independent of the microwave sensor. Microfluidic tubing was connected first to a reference flow sensor, and then to the inlet port of the device. A circulator was employed to measure the microwave resonator via single port. CPW: coplanar waveguide microwave resonator **b** Top view of

the membrane taken under an optical microscope and cross-sectional schematics (not-to-scale) of the fabricated device. The signal (SGN) and ground (GND) electrodes of the microwave resonator extend toward each other and overlap with the membrane for capacitive detection of deformation

membrane, serves as a direct means to obtain flow rates. In this case, the interaction of fluid flow with a membrane can result in nonlinear effects, such as oscillations under constant flow as reported optically in various systems before (Lammerink et al. 1995; Gervais et al. 2006; Ducloux et al. 2007; Kim et al. 2012; Xia et al. 2012, 2014; Stoecklein and Di Carlo 2018; Battat et al. 2022). Here instead of using optical means, we used an integrated microwave transducer, to electronically detect pulsations of the thin membrane, the period of which depends on flow rate. Finally, we tested the same system under applied gas pressure to draw further insight about the transduction mechanism and dynamics of membrane.

2 Experiments

We fabricated flow sensors by fabricating a coplanar wave guide (CPW) microwave resonator overlapping with a 220 nm thick membrane (Fig. 1). The microwave resonator can be modeled as an RLC circuit where the capacitance is determined by the distance between the signal and ground electrodes, as well as the amount and composition of dielectric material between the electrodes. In the case of the CPW geometry used in this work, the gap between the signal and ground electrodes was 400 μm which narrows down to 20 μm on the membrane, defining an active sensing region

which overlaps with the thin membrane (Fig. 1b). When applied pressure or fluid flow deform the thin membrane, the distance between the two electrodes, as well as the amount of matter in the proximity of the electrodes changes. These changes in turn modify the capacitance—and consequently the resonance frequency—of the microwave resonator. The changes in the resonance frequency can be tracked by a custom electronic circuit based on phase-locked loops (Kelleci et al. 2018).

The experimental setup consisted of two major subsystems: a microfluidic flow controller and an electronic measurement system (Fig. 1). The chip was placed under a microscope stage to directly observe the mechanical deformations of the membrane. To fabricate the device (Fig. 1b), we began with a commercially available wafer, consisting of 500 μm Si substrate, a 2 μm SiO₂ middle layer and a 220 nm Silicon Nitride top layer. The topmost Silicon Nitride eventually formed the membrane of interest (Figure S1a). Photolithography was performed on the backside of the wafer to define an etch window. The window was etched via inductively coupled plasma (Figure S1b) and left overnight in KOH wet etching (Figure S1c). KOH etched through Si and SiO₂, and a 220 nm thick membrane formed on the front surface. Sensors with different membrane sizes were utilized to monitor fine and coarse flow rates. The typical dimensions for the fabricated membrane are approximately 600–1500 μm in length and 300–500 μm in width.

Gold paths for defining the CPW microwave resonator were patterned on the front side of the wafer. Photolithography was performed with a mask aligned with respect to the thin film membrane (Figure S1d). Then, a 100 nm gold layer was deposited to form the signal and ground electrodes (Figure S1e). Coplanar waveguide resonator was designed to have a 50 Ω impedance to match the impedance of the electronic measurement system.

To fabricate the microfluidic channel, a negative photoresist (SU-8, Sigma-Aldrich) was used to fabricate the molds. Cured PDMS (ratio 10:1) was poured onto these molds and left to bake at 80 °C. Microchannels, typically having dimensions of 300 μm in width and 150 μm in depth, were peeled off from the mold. Through plasma cleaning process, the micro-channels were bonded on top of the chip and aligned with the membrane and gold electrodes (Figure S1f).

DI water was driven by a controllable pressure pump (MFCS-EZ, Fluigent) and passed through a commercial, thermal flow sensor (FRP, Fluigent) before reaching the microfluidic channel on the chip. The commercial flow sensor has a 430 μm ID borosilicate capillary and measures the flow rate by combining two different temperature readings obtained from two different locations inside the capillary. In between these two temperature sensors, there is a micro heater, and the flow rate value is calculated by the dissipation of the heat. The range of this commercial sensor, calibrated with water, is 0–120 $\mu\text{L}/\text{min}$, with an accuracy of 5% above 2.4 $\mu\text{L}/\text{min}$ and a 0.12 $\mu\text{L}/\text{min}$ deviation below 2.4 $\mu\text{L}/\text{min}$. PTFE tubes were used to deliver the DI water to the micro channel.

Data acquisition was conducted with a custom-built LabVIEW program where the electronic data and flow rate values from a commercial sensor were simultaneously recorded every 50 ms. To increase the sensitivity of the microwave sensor, we utilized a narrow-band detection scheme which was centered around the first resonance frequency of the CPW structure. Phase-sensitive detection was performed with a lock-in amplifier (Zurich Instruments, MFLI). Due to the upper frequency limitation of the lock-in amplifier, we constructed an external heterodyne circuitry (Ferrier et al. 2009; Nikolic-Jaric et al. 2009; Afshar et al. 2016) to continuously track the resonance frequency (Figure S2). With a phase-locked loop (PLL), the phase of the resonator was locked to 0 degrees with a PI controller (Kelleci et al. 2018). Any deviation from 0 degrees emerged as an error signal, updating the frequency of the signal generator. With this method, we could effectively keep track of the shifts in the resonance. A similar sensor without the membrane was utilized in different experiments which did not exhibit any of the fluid-related dynamics reported in this work (Secme et al. 2023). This work serves as a control experiment, indicating that the thin membrane is at the origin of the response to the applied pressure and fluid flow.

3 Experimental results

3.1 Liquid sensing

First, we characterized the membrane-based sensors using DI water. In this case, two different mechanisms emerged as a result of the interaction of the membrane with the liquid pressure/flow. These mechanisms are summarized in Fig. 2. When the pressure was first applied, the membrane responded immediately: this deformation produced a large frequency change, Δf_{target} , in the microwave resonator (e.g. 60 kHz for a set flow rate of 10 $\mu\text{L}/\text{min}$). If the pressure/flow rate on the membrane was kept constant, the membrane did not merely stay at the same equilibrium position. Rather, it exhibited quick pulsating motions that repeated with a periodicity T_{pulse} : this period depends strongly on the flow rate. As a result of these pulsations (which are typically visible under optical microscope as detailed below), the microwave resonance frequency also underwent resonance shifts, Δf_{pulse} . These frequency shifts Δf_{pulse} exhibited a weak dependency with respect to the flow rate/applied pressure in contrast to the frequency shifts caused by the initial deformation. Below, we will first report the observations on the initial deformation as a set flow rate is applied, then we will investigate the membrane pulsations.

3.2 Indirect flow rate sensing by membrane deformation

In the first experiments, we investigated the response of the device from the reset condition (where there was no fluid flow) to the target flow rate while monitoring the resonance frequency of the microwave sensor. When the pressure was first applied, the flow rate quickly climbed to the target value as observed by the commercial flow meter. At the same time, the membrane deformed (Fig. 2 b–c), and a sharp shift was observed in the resonance frequency (Fig. 3). Each of these shifts depended on the magnitude of the flow rate (Fig. 3b) through applied pressure, indicating that the amount of frequency shift can be used as a sensing parameter for the target flow rate.

The baseline frequency fluctuations were about ~ 1 kHz, from which one can extrapolate a short-term sensitivity level of 0.5 $\mu\text{L}/\text{min}$. However, as shown with the error bars of Fig. 3b, repeating the experiment with the same flow rates resulted in a dispersion in the frequency shifts with a standard deviation of 5.5 kHz which was larger than the baseline frequency noise. The sensor demonstrated here exhibited a time resolution of only several seconds when the flow rate was increased stepwise (Fig. 3c–d). When

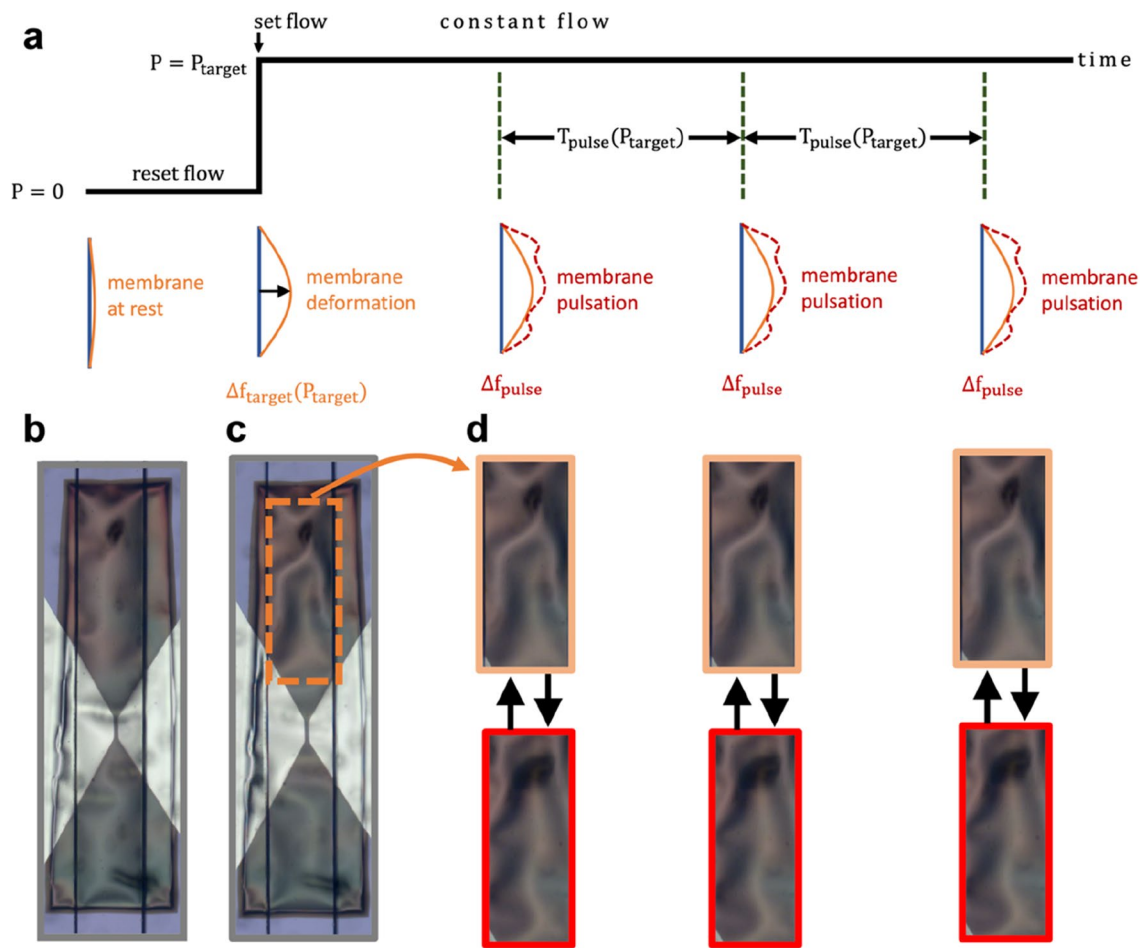


Fig. 2 Response of the device as a function of time. **a** Schematic illustration. **b–d** Micrographs of the membrane area at approximately at the same times with the time axis. When the pressure is first applied, a large deformation occurs (compare **b** with **c**) which induces a frequency shift in the microwave domain which strongly depended on the applied pressure. As the pressure is kept constant, the membrane undergoes periodic pulsations. While the duration between

these pulsations depended strongly on the applied pressure, the size of microwave frequency shift only had a weak dependence (Figure S5). Part of the membrane shuttled between different deformations states (full membrane motion can be seen in the Supplementary Video 1). The duration of these transitions depended on the fluid flow inside the microchannel. This device, device 1, has membrane dimensions were 1.5 mm length, 0.3 mm width, 220 nm thickness

the flow was stopped, we observed a downward frequency drift that lasts for approximately 50 s (Fig. 3a), however, additional flow rate measurements can still be conducted during recovery period either using successive frequency shifts (Figure S7) or by directly working with the phase shift of the resonator (as in Fig. 3c–d).

3.3 Direct flow rate sensing by periodic membrane pulsations

After the initial deformation due to applied pressure, keeping the pressure constant induces further dynamical effects in the form of dynamical instability. The interaction of thin membranes with microfluidics channels can result in dynamical bistability: indeed, oscillations of a flexible membrane under a constant input flow as demonstrated in numerous

earlier work (Lammerink et al. 1995; Gervais et al. 2006; Ducloux et al. 2007; Kim et al. 2012; Xia et al. 2012, 2014; Stoecklein and Di Carlo 2018; Battat et al. 2022). In our experiments at constant liquid flows, we observed periodic deformations of the membrane under optical microscopy as shown in Fig. 2 bottom panel, and Supplementary Video 1. These optical observations were also picked up electronically by the microwave sensor which acts as an integrated transducer on the membrane (Fig. 4). Two different configurations of the same channel were used to deduce the origin of the oscillations. In the first configuration, the output port of the microfluidic channel was kept open, so the applied pressure induced a continuous fluid flow through the channel and over the membrane. In this case, periodic pulsations clearly emerged (Fig. 4, blue trace). In the second configuration, the channel was blocked at the output port

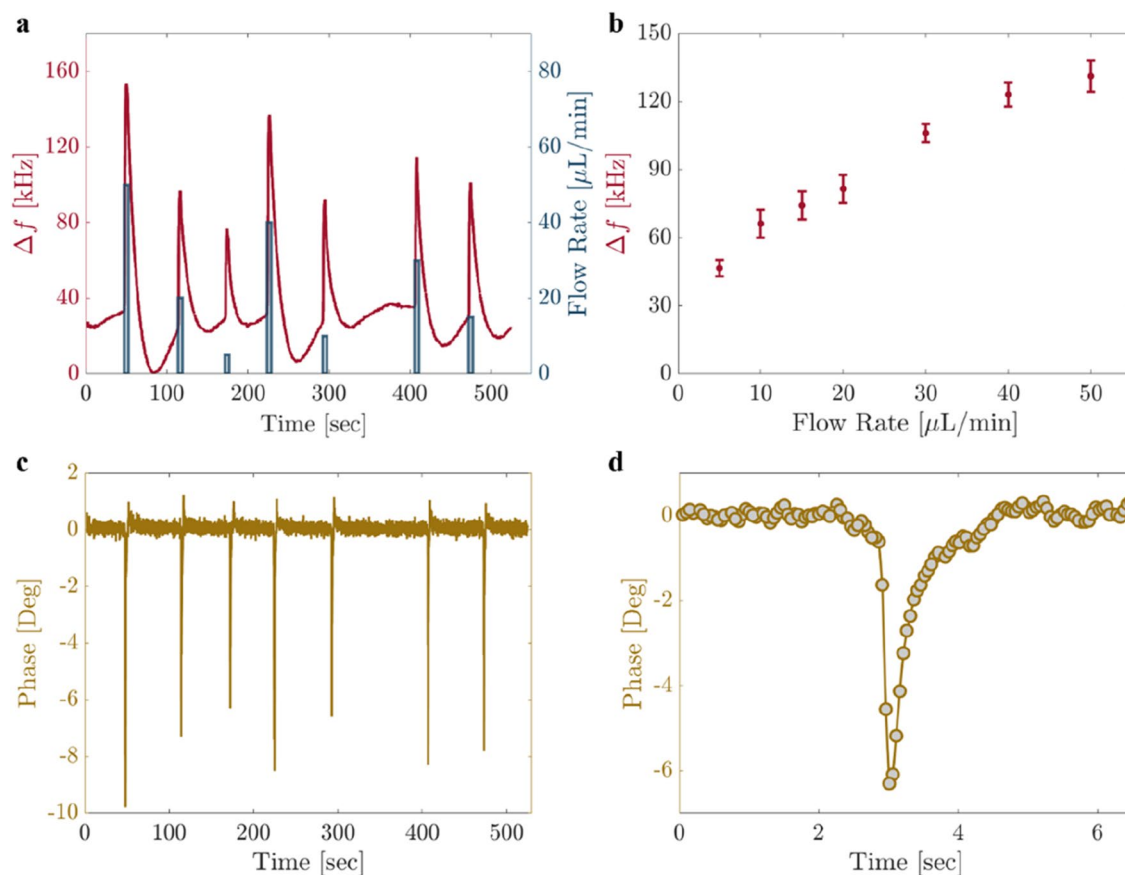


Fig. 3 **a** Frequency response of the device from the reset fluid flow. **b** Frequency shifts *versus* the target flow rate. The shifts show a monotonically increasing behavior. **c** Phase response of the data depicted in

a from the reset fluid flow condition. **d** Close-up view shows fast settling time for phase response. This device, device 2, has dimensions of 0.8 by 0.35 mm membrane area, and 0.25 mm channel width

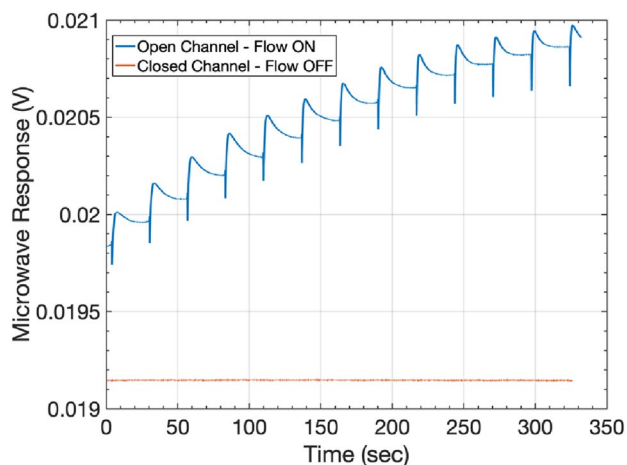


Fig. 4 The effect of flow versus pressure on the pulsation mechanism, when the output end of the microfluidic channel is kept open (blue trace) and blocked (red trace). In both cases, a pressure of 79 mBar was applied. The device used here is device 2

to prevent fluid flow. Repeating the same experiment at the same pressure, does not induce any such periodic behavior (Fig. 4, red trace). These observations, repeated for three different pressure values (65, 72 and 79 mBar) suggest that the periodic pulsations are induced by the flow of the liquid, rather than the applied pressure.

The period of the modulations depends on the fluid flow rate as illustrated in Fig. 5. The figure shows the relation between the phase response of the resonator and the effective flow rate. The commercial flow rate sensor was placed in the experimental setup (as in Fig. 1a) to set the flow rate at a constant value. In this way, the desired flow rate values were set within the limit of sensitivity of the flow meter.

In Fig. 5a, two different flow rates, 10 and 5 $\mu\text{L}/\text{min}$, were tested. For a given constant flow rate, the time between two consecutive pulses, called the pulse interval (T_i), remained constant. As the flow rate was set to a different constant value, the pulse interval changed as well. When the flow rate was set to 10 $\mu\text{L}/\text{min}$, pulse interval T_1 was approximately 7 s, whereas at a 5 $\mu\text{L}/\text{min}$ flow rate, pulse interval T_2 increased to approximately 14 s. Small peaks in the flow rate

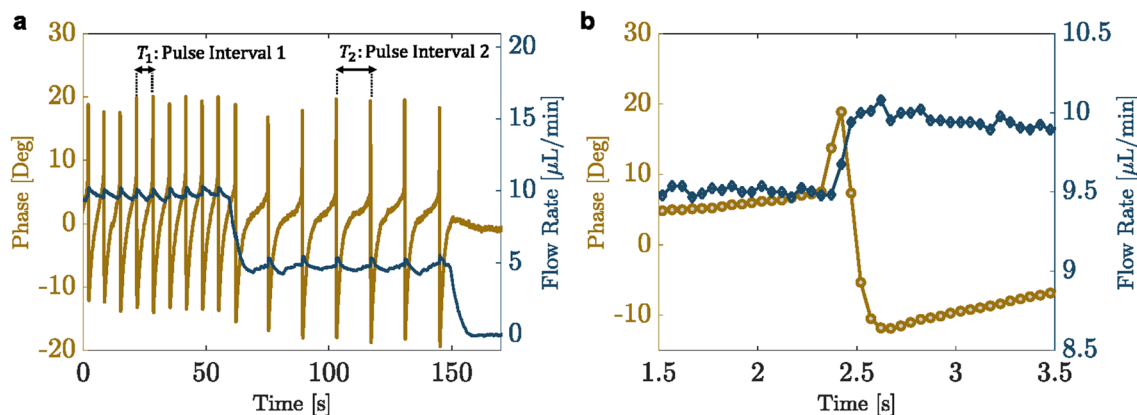


Fig. 5 **a** An example time-trace of the pulsation behavior of the sensor. The microwave response and the flow rate obtained from the reference flow sensor were measured and recorded simultaneously by LabVIEW. The pulsation periods depended on the set flow rate. **b** Close-up view of an event sequence. First, the membrane starts to

deflect inducing a change in the phase of the microwave sensor (dark yellow trace), and then a follow-up perturbation occurred in the commercial flow rate sensor (dark blue trace). The device used here is device 2.

(as measured by the commercial sensor) were observed after each pulsation (Fig. 5b). Since a deflected membrane results in an enlarged channel, the fluidic resistance decreases which in turn results in a temporary increase in the flow rate. Supplementary video 2 shows the simultaneous optical and microwave recordings of the pulsating membrane.

We note that the experiments were conducted without using any components with cyclical mechanisms such as syringe pumps: rather, the flow was induced by pressure driven sources. We also conducted control experiments where commercial flow rate sensor was removed from the system and the fluid flow was provided through a vial kept at constant pressure (as in Fig. 4, and also a separate data set in SI Table 1). In this case, where only a constant pressure

source drives the flow, we verified that membrane pulsations still occur.

After the initial observations, we used three different device geometries to span different flow rates. To enhance the sensitivity of the resonator, a large membrane (1.5 mm × 0.3 mm) was fabricated and used to resolve the slight increments in the flow rate. The resonance frequency of the microwave sensor coupled to the first membrane was 3.66 GHz. As shown in Fig. 6 (blue data points), the flow rate was set to an interval of 0–1 µL/min with an incremental change of 0.1 µL/min via the reference sensor. Until 0.3 µL/min, the device did not register any pulsation in the resonance frequency. After reaching a flow rate of 0.4 µL/min, the device began to exhibit discernible pulses. Then, the

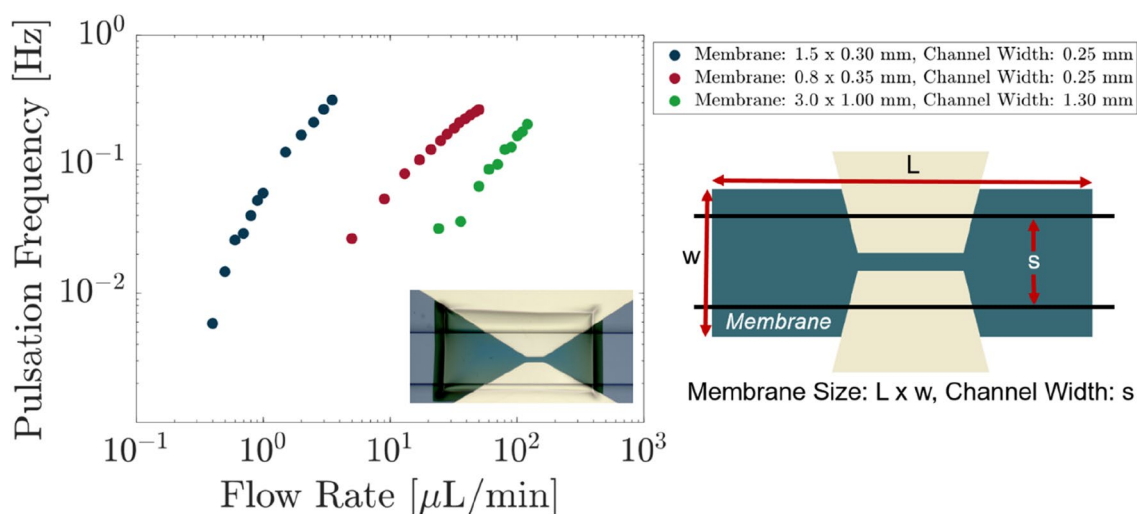


Fig. 6 Pulsation frequency as a function of flow rates for different geometries. Three different devices were used in the experiments and their dimensions are provided. In all three experiments, pulsation frequencies were observed to increase monotonically, as the flow rate was increased

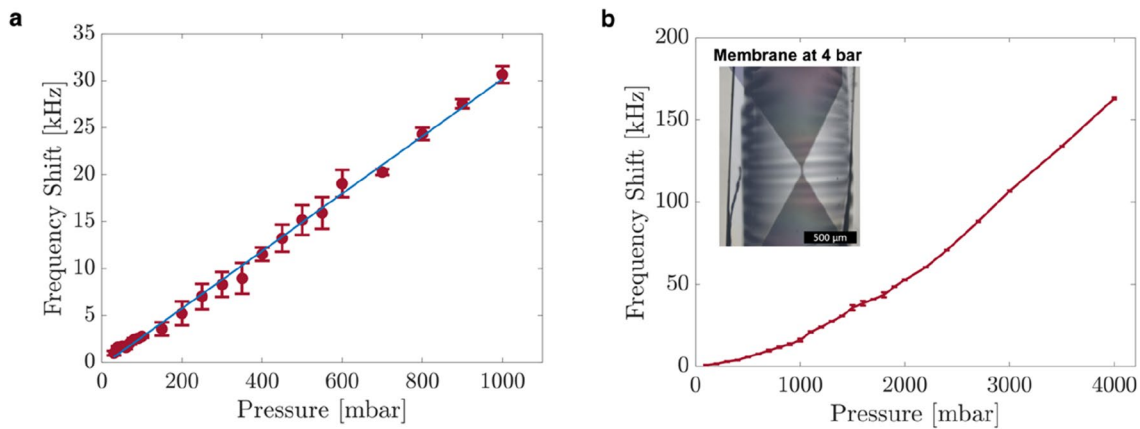


Fig. 7 Frequency response of the device from the reset fluid flow of gas. **a** The response of the membrane with 1.7 mm \times 1 mm in size coupled to a channel of 0.25 mm width. **b** The response of the membrane with 3 mm \times 1 mm in size coupled to a channel of 1.3 mm

flow rate increment was changed to 0.5 μ L/min and a range of flow rate values were tested until 3.5 μ L/min. Blue data points in Fig. 6 indicate an increasing relation between the flow rate and the frequency of the pulsation.

A second device—with membrane dimensions of 0.8 mm by 0.35 mm, and a microwave resonance frequency of 2.36 GHz—was used to span a higher flow rate range. We started from 5 μ L/min and recorded pulses for 300 s at each flow rate value. Then, the flow rate was increased with 5 μ L/min steps, reaching a flow rate of 50 μ L/min (red data points, Fig. 6). A third device—with membrane dimensions of 3 \times 1 mm, and a microwave resonance frequency of 2.08 GHz—was used to operate at higher flow rates. This device could accommodate higher flow rates, since the width of the microfluidic channel was relatively large. Starting with 24 μ L/min, we increased the flow rate until 120 μ L/min which is the upper limitation of the commercial flow sensor. We kept observing a similar trend whereby the pulsation frequency correlates with the fluid flow rate (green data points, Fig. 6).

These results indicate that membrane-integrated microwave sensors can also be used for flow sensing by detecting the period of membrane oscillations. While at high flow rates, the observed pulsations occur frequently resulting in rapid update times for flow monitoring; at low flow rates, the duration between the pulses gets longer. As a result, the update rate of the device is slow for low flow rates, which constitutes a shortcoming of this secondary flow sensing mechanism.

3.4 Gas sensing experiments

As mentioned earlier, the change in the capacitance of the resonator could originate from either the change of

width. The pressure was increased up to 4 bar and a monotonically increasing response is observed. Inset show the micrograph of the membrane and the channel when the gas inlet pressure is at 4 bar

the interelectrode separation (and similar effects of geometric origin), or the inflow of extra material near the sensing region due to the expansion of the material (or outflow of material when there is a contraction). To gain further insight about the contribution of these two sensing mechanisms, we conducted experiments with pressurized air. Since the permittivity of the air is close to the free space, the observed effects originate mainly due to the change in interelectrode separation or other deformations in the membrane geometry, rather than the effect of material flow. For the first air flow experiment, we used a membrane with dimensions of 1.7 mm length and 1 mm width within a channel width of 0.25 mm. The resonance frequency was approximately 2.55 GHz. We spanned the pressure from 20 mbar until 1000 mbar. We have seen an almost linear relationship for the higher pressure value (Fig. 7a), however, at low pressures, the trend deviated from the linear response slightly.

To work at higher air flow rates, another device was fabricated with an increased channel width of 1.3 mm (instead of 0.25 mm, in the previous device). The size of the membrane was 3 \times 1 mm and the resonance frequency of the microwave sensor was approximately 2.08 GHz. A monotonically rising frequency response was again observed as the applied pressure increased (Fig. 7b). The experiment also demonstrated that the device with 220 nm Silicon nitride membrane could endure an applied pressure up to 4 bar (Supplementary Video 3 shows the membrane deformation as the pressure is suddenly switched between the reset condition and 4 bar applied pressure).

4 Discussion

Considering the fact that the visible expansion and deformation of the membrane pressurized by air cause frequency shifts, we conclude that part of the response of the device originates from change in electrode distance and geometry. Further experimental studies are required to carefully quantify and compare the relative magnitudes of these two effects. The fact that the effective dielectric constant of the material flowing through the channel affects the resonance frequency creates a limitation for the proposed flow sensor for situations where the flow composition can change dynamically.

The amount of deformation on the membrane area can be estimated by measuring the surface topography through optical profilometry. The optical profilometry result for device 2 (the one used in Figs. 3, 4, 5) indicates dips and peaks as large as 30 μm (Supplementary Sect. 1). We used the profilometry results to estimate the size of the frequency shifts of the microwave resonators, by modeling the wrinkles as hemi-spherical, liquid-filled pocket on the membranes and conducting finite-element simulations (Supplementary Sect. 1). The simulations indicate that the expected effect is close to observed values in membrane deformation experiments (e.g. 56 kHz frequency shift for a hemi-spherical pocket with 30 μm radius). Thus, the effect of extra liquid that can be accommodated by the large deformations of the membrane appears to have a significant contribution to the full response of the microwave resonator.

Large-amplitude wrinkles and deformations of the device brings about further considerations regarding the use of the technique in lab-on-a-chip systems. While the bottom wall of the microfluidic channel undergoes large deformations, the extended membrane still stays within the volume defining the lab-on-a-chip device. The use of such large deformations is typically avoided in conventional engineering designs due to their nonlinear response of mechanical systems; however, as seen in the data here, an emergent feature of the dynamical motion—the frequency of pulsation—correlates almost linearly with the flow rates, thereby providing a robust route for flow sensing. Large-scale deformability of microfluidic components can provide further benefits (Xia et al. 2021), such as the ability to dynamically adjust a constriction size for efficient cell transfection (Alhmoud et al. 2023).

5 Conclusion

In conclusion, we demonstrated that thin membranes integrated with microwave resonators can detect flow rates of fluids. Applied pressure and/or fluid flow induce

deformations on the membrane, which in turn, modulates the capacitance of a microwave resonator. The capacitance change can be readily measured by tracking the resonance frequency of the microwave resonator. The choice of a sturdy Silicon Nitride membrane as the compliant mechanism enables the measurements of both liquid and gas flow through the same microfluidic architecture. In terms of mechanical transduction of liquid flow, in addition to the expected quasi-static deformation of the membrane, a secondary flowrate sensing mechanism emerges whereby steady flow induces periodic pulsations on the thin membrane. The pulsation period of the membrane can be sensitively measured by the changes of the phase response of the microwave sensor. For both sensing mechanisms, the high sensitivity of microwave resonators serves as a potent transducer for probing the interaction dynamics of fluid flow and thin membranes.

Supplementary Information The online version contains supplementary material available at <https://doi.org/10.1007/s10404-023-02640-9>.

Acknowledgements The authors thank John E. Sader and Jesse Collis for helpful discussions. This project has received funding from the European Research Council (ERC) under the European Union's Horizon 2020 research and innovation program (Grant agreement No 758769).

Author contributions MSH and HSP conceived the idea. HSP, AS and HDU fabricated the devices. AS, HDU, UT and HSP conducted experiments. HDU, BK, AS and CA analyzed data. HSP, HDU, AS, CA and MSH wrote the manuscript.

Data availability The datasets generated during and/or analyzed during the current study are available from the corresponding author on reasonable request.

Declarations

Conflict of interests MSH is a cofounder of Sensonance Engineering company. For other authors, there are no conflicts to declare

References

- Afshar S, Salimi E, Braasch K, Butler M, Thomson DJ, Bridges GE (2016) Multi-frequency DEP cytometer employing a microwave sensor for dielectric analysis of single cells. *IEEE Trans Microwave Theory Techn* 64(3):991–998
- Alhmoud H, Alkhaled M, Kaynak BE, Hanay MS (2023) Leveraging the elastic deformability of polydimethylsiloxane microfluidic channels for efficient intracellular delivery. *Lab Chip* 7:94
- Attia R, Pregibon DC, Doyle PS, Viovy J-L, Bartolo D (2009) Soft microflow sensors. *Lab Chip* 9(9):1213–1218
- Baldwin A, Yu L, Meng E (2016) An electrochemical impedance-based thermal flow sensor for physiological fluids. *J Microelectromech Syst* 25(6):1015–1024
- Battat S, Weitz DA, Whitesides GM (2022) Nonlinear phenomena in microfluidics. *Chem Rev* 122(7):6921–6937
- Campagnolo L, Nikolić M, Perchoux J, Lim YL, Bertling K, Loubiere K, Prat L, Rakić AD, Bosch T (2013) Flow profile measurement

- in microchannel using the optical feedback interferometry sensing technique. *Microfluid Nanofluid* 14(1–2):113–119
- Cavaniol C, Cesar W, Descroix S, Viovy J-L (2022) Flowmetering for microfluidics. *Lab Chip* 22(19):3603–3617
- Cetin AE, Stevens MM, Calistri NL, Fulciniti M, Olcum S, Kimmerling RJ, Munshi NC, Manalis SR (2017) Determining therapeutic susceptibility in multiple myeloma by single-cell mass accumulation. *Nat Commun* 8(1):1613
- Chen Z, Guo Z, Mu X, Li Q, Wu X, Fu H (2019) Packaged microbubble resonator optofluidic flow rate sensor based on Bernoulli Effect. *Opt Exp* 27(25):36932–36940
- Cheri MS, Latifi H, Sadeghi J, Moghaddam MS, Shahraki H, Hajghassem H (2014) Real-time measurement of flow rate in microfluidic devices using a cantilever-based optofluidic sensor. *Analyst* 139(2):431–438
- Christ KV, Turner KT (2010) Methods to measure the strength of cell adhesion to substrates. *J Adhes Sci Technol* 24(13–14):2027–2058
- Czarske J, Büttner L, Razik T, Müller H (2002) Boundary layer velocity measurements by a laser Doppler profile sensor with micrometre spatial resolution. *Measure Sci Technol* 13(12):1979
- Dijkstra M, de Boer MJ, Berenschot JW, Lammerink TSJ, Wiegerink RJ, Elwenspoek M (2007) Miniaturized flow sensor with planar integrated sensor structures on semicircular surface channels. In: 2007 IEEE 20th international conference on micro electro mechanical systems (MEMS). IEEE, pp 123–126
- Ducloux O, Talbi A, Gimeno L, Viard R, Pernod P, Preobrazhensky V, Merlen A (2007) Self-oscillation mode due to fluid-structure interaction in a micromechanical valve. *Appl Phys Lett* 91(3):034101
- Ejeian F, Azadi S, Razmjou A, Orooji Y, Kottapalli A, Warkiani ME, Asadnia M (2019) Design and applications of MEMS flow sensors: a review. *Sens Actu A Phys* 295:483–502
- Enoksson P, Stemme G, Stemme E (1997) A silicon resonant sensor structure for Coriolis mass-flow measurements. *J Microelectromech Syst* 6(2):119–125
- Ferrier GA, Romanuik SF, Thomson DJ, Bridges GE, Freeman MR (2009) A microwave interferometric system for simultaneous actuation and detection of single biological cells. *Lab Chip* 9(23):3406–3412
- Garstecki P, Fuerstman MJ, Stone HA, Whitesides GM (2006) Formation of droplets and bubbles in a microfluidic T-junction—scaling and mechanism of break-up. *Lab Chip* 6(3):437–446
- Gass V, van der Schoot BH, de Rooij NF (1993) Nanofluid handling by micro-flow-sensor based on drag force measurements. In: Proceedings IEEE micro electro mechanical systems. IEEE, Fort Lauderdale, FL, USA, pp 167–172. <https://doi.org/10.1109/MEMSYS.1993.296928>
- Gervais T, El-Ali J, Günther A, Jensen KF (2006) Flow-induced deformation of shallow microfluidic channels. *Lab Chip* 6(4):500–507
- Glawdel T, Elbuken C, Ren CL (2012) Droplet formation in microfluidic T-junction generators operating in the transitional regime. I. Experimental observations. *Phys Rev E* 85(1):016322
- Haneveld J, Lammerink TS, de Boer MJ, Sanders RG, Mehendale A, Lötters JC, Dijkstra M, Wiegerink RJ (2010) Modeling, design, fabrication and characterization of a micro Coriolis mass flow sensor. *J Micromech Microeng* 20(12):125001
- Harink B, Le Gac S, Truckenmüller R, van Blitterswijk C, Habibovic P (2013) Regeneration-on-a-chip? The perspectives on use of microfluidics in regenerative medicine. *Lab Chip* 13(18):3512–3528
- Kelleci M, Aydogmus H, Aslanbas L, Erbil SO, Hanay MS (2018) Towards microwave imaging of cells. *Lab Chip* 18(3):463–472
- Kim J, Cho H, Han S-I, Han A, Han K-H (2019) A disposable microfluidic flow sensor with a reusable sensing substrate. *Sens Actu B Chem* 288:147–154
- Kim S-J, Yokokawa R, Leshner-Perez SC, Takayama S (2012) Constant flow-driven microfluidic oscillator for different duty cycles. *Analyst Chem* 84(2):1152–1156
- Kuo JT, Yu L, Meng E (2012) Micromachined thermal flow sensors—a review. *Micromachines* 3(3):550–573
- Lammerink TSJ, Tas NR, Berenschot JW, Elwenspoek MC, Fluitman JHJ (1995) Micromachined hydraulic astable multivibrator. In: Proceedings IEEE micro electro mechanical systems. Citeseer, p 13
- Lin W-C, Burns MA (2015) Low-power micro-fabricated liquid flow-rate sensor. *Analyst Methods* 7(9):3981–3987
- Maenhout G, Bao J, Markovic T, Ocket I, Nauwelaers B (2019) Reliable, fast and reusable interfacing of high-frequency signals to disposable lab-on-a-chip devices. In: 2019 IEEE MTT-S international microwave biomedical conference (IMBioC). IEEE, pp 1–4
- Mehling M, Tay S (2014) Microfluidic cell culture. *Curr Opin Biotechnol* 25:95–102
- Nguyen N (1997) Micromachined flow sensors—A review. *Flow Measure Instrument* 8(1):7–16
- Nikolic-Jaric M, Romanuik S, Ferrier G, Bridges G, Butler M, Sunley K, Thomson D, Freeman M (2009) Microwave frequency sensor for detection of biological cells in microfluidic channels. *Biomicrofluidics* 3(3):034103
- Noeth N, Keller SS, Boisen A (2014) Integrated cantilever-based flow sensors with tunable sensitivity for in-line monitoring of flow fluctuations in microfluidic systems. *Sensors* 14(1):229–244
- Oosterbroek R, Lammerink TS, Berenschot JW, Krijnen GJ, Elwenspoek MC, van den Berg A (1999) A micromachined pressure/flow-sensor. *Sens Actu A Phys* 77(3):167–177
- Salipante P, Hudson SD, Schmidt JW, Wright JD (2017) Microparticle tracking velocimetry as a tool for microfluidic flow measurements. *Exp Fluids* 58(7):85
- Secme A, Tefek U, Sari B, Pisheh HS, Uslu HD, Akbulut O, Kucukoglu B, Erdogan RT, Alhmodh H, Sahin O (2023) High resolution dielectric characterization of single cells and microparticles using integrated microfluidic microwave sensors. *IEEE Sens J*. <https://doi.org/10.1109/JSEN.2023.3250401>
- Stern L, Bakal A, Tzur M, Veinguer M, Mazurski N, Cohen N, Levy U (2014) Doppler-based flow rate sensing in microfluidic channels. *Sensors* 14(9):16799–16807
- Stevens MM, Maire CL, Chou N, Murakami MA, Knoff DS, Kikuchi Y, Kimmerling RJ, Liu H, Haidar S, Calistri NL (2016) Drug sensitivity of single cancer cells is predicted by changes in mass accumulation rate. *Nat Biotechnol* 34(11):1161–1167
- Stoecklein D, Di Carlo D (2018) Nonlinear microfluidics. *Analyst Chem* 91(1):296–314
- Tang M, Liu F, Lei J, Ai Z, Hong S-L, Zhang N, Liu K (2019) Simple and convenient microfluidic flow rate measurement based on microbubble image velocimetry. *Microfluid Nanofluid* 23(11):118
- Temiz Y, Delamarche E (2018) Sub-nanoliter, real-time flow monitoring in microfluidic chips using a portable device and smartphone. *Sci Rep* 8(1):1–11
- Ward T, Faivre M, Abkarian M, Stone HA (2005) Microfluidic flow focusing: drop size and scaling in pressure versus flow-rate-driven pumping. *Electrophoresis* 26(19):3716–3724
- Węglarski M, Jankowski-Mihułowicz P, Pitera G, Jurków D, Dorczyński M (2020) LTCC flow sensor with RFID interface. *Sensors* 20(1):268
- Wexler JS, Trinh PH, Berthet H, Quennou N, Du Roure O, Huppert HE, Lindner A, Stone HA (2013) Bending of elastic fibres in viscous flows: the influence of confinement. *J Fluid Mech* 720:517–544
- Wissman JP, Sampath K, Freeman SE, Rohde CA (2019) Capacitive bio-inspired flow sensing cupula. *Sensors* 19(11):2639
- Wu LY, Di Carlo D, Lee LP (2008) Microfluidic self-assembly of tumor spheroids for anticancer drug discovery. *Biomed Microdev* 10(2):197–202
- Xia H, Wang Z, Fan W, Wijaya A, Wang W, Wang Z (2012) Converting steady laminar flow to oscillatory flow through a hydroelasticity approach at microscales. *Lab Chip* 12(1):60–64

- Xia H, Wang Z, Nguyen V, Ng S, Wang W, Leong F, Le D (2014) Analyzing the transition pressure and viscosity limit of a hydroelastic microfluidic oscillator. *Appl Phys Lett* 104(2):024101
- Xia H, Wu J, Zheng J, Zhang J, Wang Z (2021) Nonlinear microfluidics: device physics, functions, and applications. *Lab Chip* 21(7):1241–1268
- Zarifi MH, Sadabadi H, Hejazi SH, Daneshmand M, Sanati-Nezhad A (2018) Noncontact and nonintrusive microwave-microfluidic flow sensor for energy and biomedical engineering. *Sci Rep* 8(1):1–10
- Zhou J, Mukherjee P, Gao H, Luan Q, Papautsky I (2019) Label-free microfluidic sorting of microparticles. *APL Bioeng.* 3(4):041504

Publisher's Note Springer Nature remains neutral with regard to jurisdictional claims in published maps and institutional affiliations.

Springer Nature or its licensor (e.g. a society or other partner) holds exclusive rights to this article under a publishing agreement with the author(s) or other rightsholder(s); author self-archiving of the accepted manuscript version of this article is solely governed by the terms of such publishing agreement and applicable law.